Rev. Roum. Sci. Techn.– Électrotechn. et Énerg.
Vol. **70**, *3*, pp. 319–324, Bucarest, 2025

PREDICTIVE DIRECT POWER CONTROL OF NEUTRAL-POINT CLAMPED CONVERTER IN WIND TURBINE SYSTEM WITH DUAL THREE-PHASE PERMANENT MAGNET SYNCHRONOUS GENERATOR

YAZID MADI[1,2], ABDELHAKIM DENDOUGA[1], DJAMAL AOUZELLAG[2]

Keywords: Three-level neutral-point clamped (NPC) converter; Dual three-phase (DTP); Permanent magnet synchronous generator (PMSG); Wind turbine; Maximum power point tracking (MPPT); Direct power control (DPC); Finite control-set model predictive direct power control (FCS-MPC-DPC).

This paper presents a predictive direct power control (DPC) of a three-phase neutral-point-clamped (NPC) converter in a wind power system based on a dual three-phase (DTP) permanent-magnet synchronous generator (PMSG). As the power in wind turbine systems increases, using a three-level NPC converter offers several advantages, including higher output power, reduced stress on semiconductor devices, and lower harmonic distortion in the output waveform, when compared to a conventional two-level converter. In the production system, a DTP PMSG is used. This generator is coupled with two three-phase, two-level voltage source converters, arranged in series to create a cascaded DC link. For interfacing with the electrical grid, the system utilizes a three-phase NPC converter. The proposed control technique uses two decoupled control loops: a field-oriented control FOC to achieve maximum power point tracking MPPT on the machine-side converters, and a finite control-set model predictive direct power control (FCS-MPC-DPC) for the NPC converter. The objectives include the tracking of active power, reactive power, and voltage balancing. The system's performance is evaluated through MATLAB/Simulink simulations.

1. INTRODUCTION

As the world grapples with the growing threat of climate change, renewable energy has emerged as a leading solution to mitigate its effects. Consequently, countries around the world are expanding their use. By 2030, renewable energy sources are predicted to generate three times as much electricity as current levels, with an expected output of 11000 GW [1]. Out of all renewable energy sources, wind power has seen the most rapid and impactful growth in recent years, with systems scaling up dramatically in size and power capacity. In the 1980s, wind turbines typically had blades of around 20 meters in diameter and capacities between 20-60 kW. Today, diameters approach or exceed 200 meters. Furthermore, the rated capacity of offshore wind power installations has already achieved maximum values ranging from 14 MW to 16 MW [2].

Wind turbines predominantly utilize two categories of electrical generators: the permanent magnet synchronous generator (PMSG) and the doubly fed induction generator (DFIG). The PMSG offers several key advantages over the DFIG [3]. Notably, the PMSG can be implemented as a direct-drive system without requiring a gearbox. Eliminating the gearbox significantly reduces the weight, mechanical losses, and maintenance needs. Thanks to these beneficial properties, the PMSG has become the predominant generator technology used in wind turbines [4]. In the past few decades, there has been an increased emphasis on research related to multi-phase machines. Multi-phase motors are finding applications in high-power electric drive systems such as electric vehicles, more electric aircraft, and ship propulsion [5-7]. These types of machines, which capable of operating in degraded mode [8], have aroused great interest due to their potential benefits for powering large-scale electric propulsion systems across various transportation sectors. Despite the existing research, multi-phase machines continue to be a compelling area of study, especially when it comes to their potential use in wind power generation applications.

Wind turbines operating at variable speeds and equipped with multiphase generators necessitate the use of three-phase power converters, which can be connected either in parallel or in series. While the parallel connection of converters enhances fault tolerance and increases robustness of the variable speed wind energy system, this configuration can lead to current imbalances between the different three-phase sets, causing additional voltages and harmful vibrations [9,10]. Moreover, if one three-phase set has no current, the currents related to switching harmonics increase in the other sets, leading to asymmetrical operation of the machine [11]. To avoid these imbalances and asymmetries, a more complex control scheme with multiple separate PI controllers for each three-phase set is required, adding complexity to the overall system [12].

Furthermore, the cross-coupling magnetic effects between the d and q axes, as well as the mutual leakage inductances between the three-phase windings, must be taken into account in the modeling and control. The series connection of the DTP machine-side converters requires only half of the total required DC-link voltage for each individual converter. The (*dv/dt)* of the common-mode voltage (CMV), recognized as a major cause of leakage currents in high-power applications, is consequently also divided by two. This, in turn, leads to a significant decrease in leakage currents, which is particularly beneficial in high-power applications where these currents can cause various issues, such as electromagnetic interference (EMI) and reduced efficiency [13]. However, there are still technological challenges around improving the reliability, efficiency and cost-effectiveness of wind energy systems. An area attracting growing research attention has been multi-phase PMSG connected to the grid via multi-level converters for large-scale wind turbines [14,15]. NPC converters are ideal for wind systems using DTP PMSG generators [16, 17]. Due to their low harmonic distortion, low electromagnetic interference, and high efficiency, they are suitable for medium and high-power applications requiring better power quality. Unlike two-level topologies, the elimination of low-frequency harmonics helps reduce

[1] Laboratoire d'Identification, Commande, Contrôle et Communication, Faculté des Sciences et de la Technologie, Université de Biskra, Algérie.
[2] Laboratoire de Maitrise des Energies Renouvelables, Faculté de Technologie, Université de Bejaia, 06000 Bejaia, Algérie.
E-mails: yazid.madi@univ-biskra.dz, a.dendouga@univ-biskra.dz, djamal.aouzellag@univ-bejaia.dz

DOI: 10.59277/RRST-EE.2025.70.3.6

the size of AC output inductors [18].

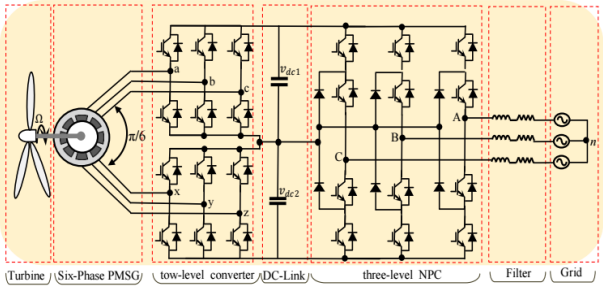

Fig. 1 – DTP PMSG connected to the grid through two-series three-phase converters and an NPC converter.

A multilevel converter-fed power conversion system is highly nonlinear, for three-level NPC converters when considering neutral point voltage balancing [19]. From a conceptual point of view, the analysis and control of such a system can be simplified by making it linear through the use of a modulator. This can limit the performance of the system [20]. In order to address the challenges associated with controlling multilevel converters such as three-level NPC, which are inherently nonlinear systems, the finite control set model predictive control (FCS-MPC) is a novel approach [21]. The principle of (FCS-MPC) is to explicitly consider the discrete states of the converter and evaluate each potential state in a cost function tailored to the desired control objectives. The optimal state that minimizes this cost function is then applied.

The main points of this paper are organized as follows. In section 2, description and modeling of the studied system, include the turbine power, the principle of maximum power point tracking (MPPT) and the DTP PMSG. Vector control of a DTP PMSG has been discussed in section 3. Section 4, direct power control (DPC) using a finite control-set model predictive control (FCS-MPC) for three-level NPC converter is presented. Section 5, this section elaborates on the discussion of the simulation results, and finally, this paper is concluded by Section 6.

2. MODELING OF THE WIND SYSTEM

The variable speed wind energy conversion system shown in Fig. 1 is composed of a wind turbine driving a DTP PMSG connected to the grid through back-to-back power converter. Two series connected three-phase converters at the generator side, and a single three-level NPC converter on the grid side. Both converters utilize the same DC-link for power exchange.

2.1 WIND TURBINE MODEL

A wind energy conversion system essentially consists of a wind turbine and an electrical generator. The wind turbine captures the kinetic energy of the wind through its blades and transmits this mechanical power to the rotor of the generator, which then converts it into electricity. Wind energy's power, expressed as the rate of kinetic energy transfer, is calculated using the following equation:

$$P_\omega = \frac{1}{2}\rho A V_\omega^3. \quad (1)$$

where, P_ω is the potentially available power in the wind, it can be observed that the wind power increases with the cube of the wind speed V_ω, implying that a modest increase in wind speed leads to a substantial increase in wind power, ρ is the air density, A is the swept area of the wind turbine rotor ($A = \pi R^2$, R is the length of the blade).

The link between the wind speed and power captured by turbine blade to convert into mechanical energy can be described as follows [22].

$$P_{tur} = \frac{1}{2} C_P(\lambda, \beta)\rho A V_\omega^3. \quad (2)$$

The speed ratio λ, which indicates the ratio between the turbine rotational speed Ω and the wind speed V_ω, is given by the following expression:

$$\lambda = \frac{R\Omega}{V_\omega}. \quad (3)$$

C_p is the power coefficient; it depends on the speed ratio λ and the blade pitch angle β. Can be approximated as follows [23]:

$$C_p(\lambda, \beta) = 0.5176\left(\frac{116}{\lambda'} - 0.4\beta - 5\right)e^{\frac{-21}{\lambda'}} + 0.0068\lambda, \quad (4)$$

With,

$$\frac{1}{\lambda'} = \frac{1}{\lambda + 0.08\beta} - \frac{0.035}{\beta^3 + 1}. \quad (5)$$

The aerodynamic torque T_{tur} of the wind turbine is given by the ratio of the power captured by turbine P_{tur}, to the turbine's rotational speed Ω, according to the following expression:

$$T_{tur} = \frac{P_{tur}}{\Omega} = \frac{1}{2}\rho\pi\frac{R^3}{\lambda}C_p(\lambda, \beta)V_\omega^2. \quad (6)$$

2.2 MPPT CONTROL

Maximum Power Point Tracking (MPPT) optimizes energy extraction in wind turbine systems. The objective of MPPT is to operate the turbine at the optimal tip speed ratio λopt and blade pitch angle that yields the maximum attainable power coefficient (Cp_max). The block diagram of the MPPT algorithm is shown in Fig. 2. The rotational speed control uses a PI controller as defined by:

$$T_{em\_ref} = \left(k_p + \frac{k_i}{s}\right)(\Omega_{ref} - \Omega). \quad (7)$$

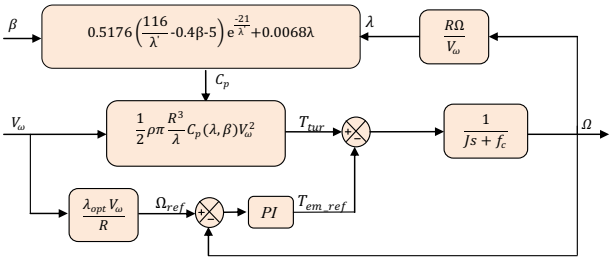

Fig. 2– MPPT Strategy with speed controller.

2.3 DTP PMSG MODEL

The asymmetric DTP permanent magnet synchronous generator has two groups of three-phase windings, with each group spatially displaced by π/6 electrical degrees, and each group having its own isolated neutral point. The basic stator voltage and flux linkage can be written as:

$$\begin{cases} v_s = R_s i_s + \frac{d}{dt}\psi_s \\ \psi_s = L_s i_s + \psi_{fs} \end{cases}, \quad (8)$$

with,

$$\psi_{fs} = \psi_{PM}\begin{bmatrix} \cos(\theta) & \cos\left(\theta-\frac{2\pi}{3}\right) & \cos\left(\theta-\frac{4\pi}{3}\right) \\ \cos\left(\theta-\frac{\pi}{6}\right) & \cos\left(\theta-\frac{5\pi}{6}\right) & \cos\left(\theta-\frac{3\pi}{2}\right) \end{bmatrix}. \quad (9)$$

where, v_s, i_s, R_s, ψ_s and ψ_{PM} are the stator voltage, current, resistance, linkage, permanent magnet flux linkage, respectively. This section presents the mathematical model of a DTP PMSG in natural coordinates, expressed as equation (8), by applying the space vector decoupling theory VSD [24]. The fundamental principle consists of decomposing the DTP PMSG system, initially represented in a six-dimensional space, into a vector space composed of three mutually orthogonal subspaces.

- Electromechanical conversion subspace (α-β): this subspace directly controls the conversion between electrical energy and mechanical torque.
- Air gap subspace (z_1-z_2): This subspace has no influence on the motor's torque generation
- (o_1-o_2) subspace: Due to the isolated neutral points, this subspace equals zero.

The VSD transformation matrix is expressed as:

$$\begin{matrix} \\ \alpha \\ \beta \\ z_1 \\ z_2 \\ o_1 \\ o_2 \end{matrix}\left[T_{\alpha\beta}\right] = \frac{1}{\sqrt{3}}\begin{bmatrix} 1 & -\frac{1}{2} & -\frac{1}{2} & \frac{\sqrt{3}}{2} & -\frac{\sqrt{3}}{2} & 0 \\ 0 & \frac{\sqrt{3}}{2} & -\frac{\sqrt{3}}{2} & \frac{1}{2} & \frac{1}{2} & -1 \\ 1 & -\frac{1}{2} & -\frac{1}{2} & -\frac{\sqrt{3}}{2} & \frac{\sqrt{3}}{2} & 0 \\ 0 & -\frac{\sqrt{3}}{2} & \frac{\sqrt{3}}{2} & \frac{1}{2} & \frac{1}{2} & -1 \\ 1 & 1 & 1 & 0 & 0 & 0 \\ 0 & 0 & 0 & 1 & 1 & 1 \end{bmatrix}. \quad (10)$$

Only the (α-β) subspace requires a rotational coordinate transformation, while the (z_1-z_2) subspace remains unchanged. The rotation transformation matrix is:

$$\left[T_{dq}\right]_{4x4} = \begin{bmatrix} cos(\theta) & sin(\theta) & 0 & 0 \\ -sin(\theta) & cos(\theta) & 0 & 0 \\ 0 & 0 & 1 & 0 \\ 0 & 0 & 0 & 1 \end{bmatrix}. \quad (11)$$

The voltage equation can be expressed in the new reference frame as:

$$\begin{cases} \frac{d}{dt}i_d = \frac{1}{L_d}\left(-R_s i_d + \omega_r L_q i_q + V_d\right) \\ \frac{d}{dt}i_q = \frac{1}{L_q}\left(-R_s i_q - \omega_r\left(L_d i_d + \sqrt{3}\psi_{PM}\right) + V_q\right) \\ \frac{d}{dt}i_{z1} = \frac{1}{L_l}\left(-R_s i_{z1} + V_{z1}\right) \\ \frac{d}{dt}i_{z2} = \frac{1}{L_l}\left(-R_s i_{z2} + V_{z2}\right) \end{cases}. \quad (12)$$

where, (Ld, Lq) are direct and quadrature inductance, Ll is the stator leakage inductance.

The electromagnetic torque generated by the component of the (d-q) subspace is represented by the following expression:

$$T_{em} = \sqrt{3}P\left(i_q\psi_{PM} + \left(L_d - L_q\right)i_d i_q\right). \quad (13)$$

where, P is the number of pole pairs.

3. VECTOR CONTROL OF THE DTP PMSG

The overall control structure of the DTP PMSG is realized through the field-oriented control (FOC) technique adapted for multiphase machine drives [25]. Utilizing two nested loops. The outer loop regulates the rotational speed of the wind turbine, while the inner loop controls the quadrature axis current. PI controllers are used, with zero reference values for the direct and homopolar axes Fig. 3. However, for a DTP PMSG with non-salient poles (Ld=Lq); electromagnetic torque will solely depend on the quadrature current iq as expressed bellow.

$$T_{em} = \sqrt{3}P\left(i_q\psi_{PM}\right) = Ki_q. \quad (14)$$

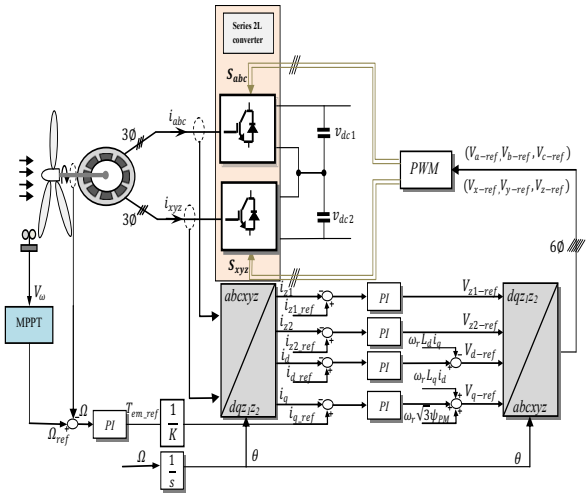

Fig. 3– Control diagram of DTP PMSG.

4. PREDICTIVE CONTROL FCS-MPC-DPC OF THE THREE-LEVEL NPC CONVERTER

The line voltage and current of the three-level NPC converter are measured and transformed into (α-β) static coordinates. The instantaneous active and reactive powers can then be expressed as [26]:

$$P = v_\alpha i_\alpha + v_\beta i_\beta\,, \quad (15)$$

$$Q = v_\beta i_\alpha - v_\alpha i_\beta. \quad (16)$$

Using a *PI* controller, the reference value of active power is generated by comparing the DC-link voltage to a desired reference value. To achieve a unity power factor, the reference value for reactive power is set to zero. Since this converter is a first-order system, it is possible to predict the values of active and reactive powers using the Forward Euler approach, as follows:

$$\frac{dP}{dt} = \frac{P(k+1) - P(k)}{T_s}, \quad (17)$$

$$\frac{dQ}{dt} = \frac{Q(k+1) - Q(k)}{T_s}. \quad (18)$$

By substituting (15) and (16) into (17) and (18):

$$\frac{P(k+1) - P(k)}{T_s} = A, \quad (19)$$

$$\frac{Q(k+1) - Q(k)}{T_s} = B. \quad (20)$$

where,

$$A = \frac{dv_\alpha}{dt}i_\alpha + \frac{di_\alpha}{dt}v_\alpha + \frac{dv_\beta}{dt}i_\beta + \frac{di_\beta}{dt}v_\beta, \quad (21)$$

$$B = \frac{dv_\beta}{dt}i_\alpha + \frac{di_\alpha}{dt}v_\beta - \frac{dv_\alpha}{dt}i_\beta - \frac{di_\beta}{dt}v_\alpha. \quad (22)$$

These derivations ($\frac{di_\alpha}{dt}, \frac{di_\beta}{dt}$) could be replaced with the system elements as follows:

$$\frac{d}{dt}\begin{bmatrix} i_\alpha \\ i_\beta \end{bmatrix} = \frac{1}{L}\left(\begin{bmatrix} v_\alpha \\ v_\beta \end{bmatrix} - R\begin{bmatrix} i_\alpha \\ i_\beta \end{bmatrix} - \begin{bmatrix} V_\alpha \\ V_\beta \end{bmatrix}\right). \quad (23)$$

where (V_α, V_β) are the average AC side voltages of the three-level NPC converter into (α-β) static coordinates. Assuming the line voltage is a balanced and pure sine wave

therefore implies that:

$$\frac{dv_\alpha}{dt} = -\omega v_\beta, \tag{24}$$

$$\frac{dv_\beta}{dt} = \omega v_\alpha. \tag{25}$$

By substituting eq. (23), (24) and (25) into (21) and (22):

$$A = v_\alpha\left(\frac{1}{L}(v_\alpha - V_\alpha - Ri_\alpha) + \omega i_\beta\right) + v_\beta\left(\frac{1}{L}(v_\beta - V_\beta - Ri_\beta) + \omega i_\alpha\right), \tag{26}$$

$$B = v_\alpha\left(\omega i_\alpha - \frac{1}{L}(v_\beta - V_\beta - Ri_\beta)\right) + v_\beta\left(\frac{1}{L}(v_\alpha - V_\alpha - Ri_\alpha) + \omega i_\beta\right). \tag{27}$$

The variation of active and reactive powers over the next sampling interval T_s is obtained as follows:

$$P(k+1) = T_s A + P(k), \tag{28}$$

$$Q(k+1) = T_s B + Q(k). \tag{29}$$

The following equations represent the voltage of each capacitor C of the DC-link over a sampling period T_s [27]:

$$v_{dc1}(k+1) = v_{dc1}(k) + \frac{1}{C} i_{c1}(k) T_s,. \tag{30}$$

$$v_{dc2}(k+1) = v_{dc2}(k) + \frac{1}{C} i_{c2}(k) T_s. \tag{31}$$

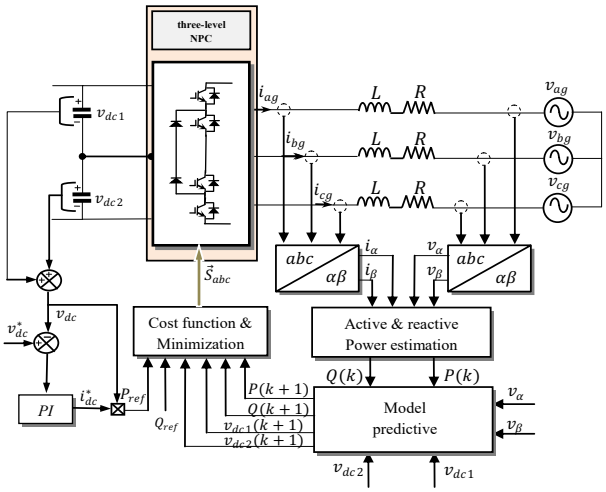

Fig. 4– Block diagram of the FCS-MPC-DPC of three-level NPC converter.

Figure 4 presents a diagram summarizing the implemented control strategy. The future values of the active power $P(k+1)$, reactive power $Q(k+1)$ and voltages in the capacitors ($v_{dc1}(k+1)$ and $v_{dc2}(k+1)$) are predicted for the 27 switching states generated by the converter. The cost function for a three-level NPC converter to achieve control targets, including active and reactive power references and neutral point voltage balancing, can be designed as:

$$g_{opt} = |P_{ref} - P(k+1)| + |Q_{ref} - Q(k+1)| + \lambda_{dc}|v_{dc1}(k+1) - v_{dc2}(k+1)|. \tag{32}$$

5. SIMULATION RESULTS

The efficiency of the proposed wind energy production system based on FCS-MPC-DPC control is studied using Matlab/Simulink software, to evaluate its performance considering the wind speed distribution shown in Fig. 5. The parameters for the proposed system are listed in Table 1.

Table 1

Parameters of the proposed system

Parameter		Unit
Rated power	2	MW
Number of pole pairs, P	26	-
d axis inductance, L_d	5.14	mH
q axis inductance, L_q	5.14	mH
Parameter		Unit
Stator leakage inductance , L_l	2.3146	mH
Stator phase winding resistance, R_s	11.6528e-3	Ohm
DC-link voltage	5300	V
C_{c1} , C_{c2}	1768.5e-5	F
Rated phase voltage, v_g (rms)	1732.1	V
Rated current, i_g (rms)	577.4	A

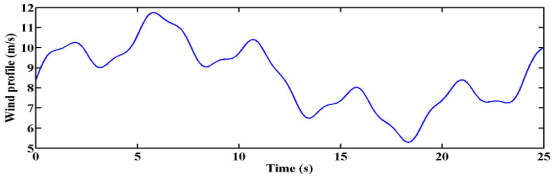

Fig. 5 – Wind profile.

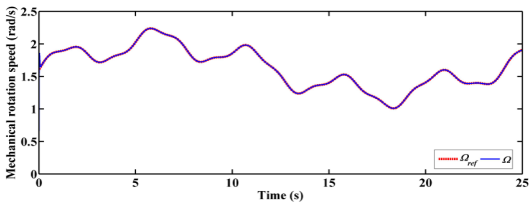

Fig. 6 – Mechanical rotation speed (Ω and Ω_{ref}).

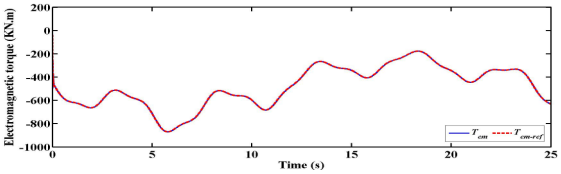

Fig. 7 – Electromagnetic torque (T_{em} and T_{em_ref}).

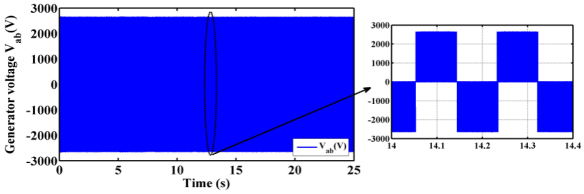

Fig. 8 – Machine-side converter output line to line voltage (V_{ab}).

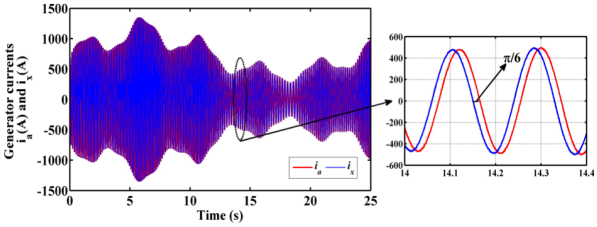

Fig. 9 – Generator currents (i_a and i_x).

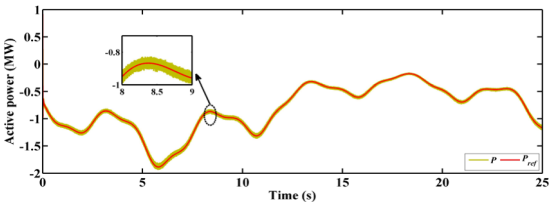

Fig. 10 – Active power transmitted to the grid (P and P_{ref}).

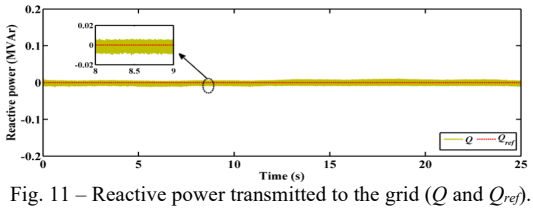

Fig. 11 – Reactive power transmitted to the grid (Q and Q_{ref}).

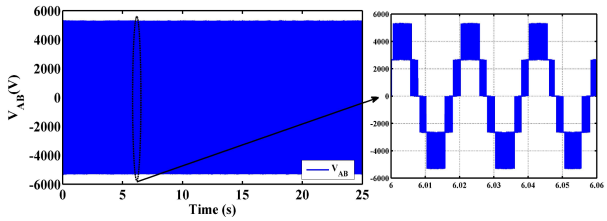

Fig. 12 – Output voltage of the three-level NPC converter (V_{AB}).

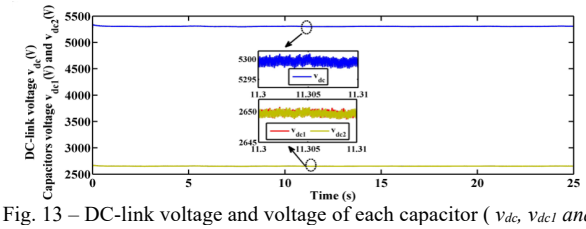

Fig. 13 – DC-link voltage and voltage of each capacitor (v_{dc}, v_{dc1} *and* v_{dc2}).

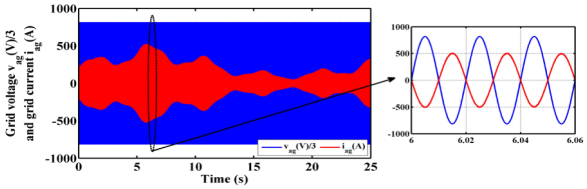

Fig. 14 – Grid voltage and grid current (v_{ag}/3 and i_{ag}).

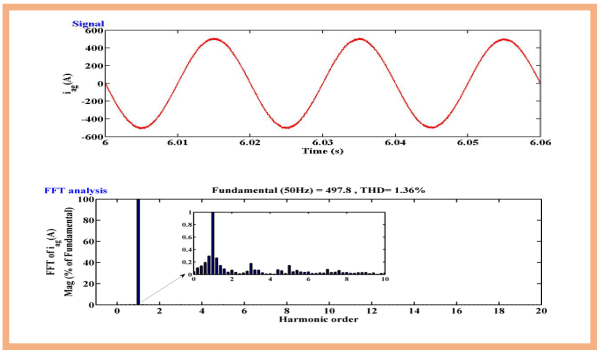

Fig. 15 – FFT of grid current i_{ag}.

Figures 6 to 9 present the speed control of the DTP PMSG using field-oriented control (FOC), where the reference speed is generated by a PI regulator based on MPPT. The figures illustrate the variation of electromagnetic torque with wind speed, the line-to-line output voltage of the machine-side converter, and the phase currents, showing a π/6 phase shift between the two sets of stator windings.

Figures 10 to 15 show the simulation results of the FCS-MPC-DPC strategy applied to the three-level NPC converter. The active and reactive powers track their references accurately, the DC-link voltage is well-regulated at 5300 V, and the capacitor voltages are maintained at 2650 V. The output voltage, grid voltage, and injected phase current confirm near-unity power factor operation. A low total harmonic distortion (THD) of 1.36% indicates a nearly sinusoidal current waveform. Table 2 compares several control techniques applied to different generators, considering their THD and the types of converters used. The THD proposed method stands out with the lowest THD (1.36%) and superior performance.

Table 2

Performance comparison.

References	Techniques	Generators	THD current grid (%)	Back-to-back Converters	Performance
[17]	(PI and HC)-(PI VOC)	DTP-PMSG	-	Dual Boost Conv-3L NPC	Low
[28]	(BSC control)-(PI VOC)	DSIG	2,60	Parallel 2L Conv-2L Conv	Medium-Low
[29]	(DBCC)-(M^{2}PCC)	Six-phase PMSG	2,06	3C Boost Conv-2C Conv	Medium - high
Proposed technique	(PI FOC)-(FCS-MPC-DPC)	DTP-PMSG	1,36	Series 2L Conv -3L NPC	High

6. CONCLUSION

In this paper, a predictive direct power control DPC has been developed for a three-phase NPC converter in a 2MW DTP PMSG wind energy conversion system. The MPPT control applied to the wind turbine and the vector control FOC applied to the DTP PMSG demonstrate an excellent ability to maintain and control electrical and mechanical parameters with minimal variations that are entirely satisfactory given the high power of the studied system. The application of direct power control DPC using finite control set model predictive control (FCS-MPC-DPC) to the three-level NPC converter has demonstrated promising results. This approach has achieved optimal grid connection, thus meeting the main objectives set by the cost function. Notably, the system excelled in accurately tracking active and reactive powers references, ensuring efficient management of the produced energy as well as the quality of the three-phase electrical current waveforms injected into the grid, and operation with a power factor close to unity. Furthermore, the neutral point voltage balancing was maintained satisfactorily, contributing to the overall stability and reliability of the system. These results highlight the effectiveness of the FCS-MPC-DPC method in improving the performance of the studied wind energy conversion system.

CREDIT AUTHORSHIP CONTRIBUTION STATEMENT

Yazid Madi: Conducted the literature review, developed the program, organized the manuscript, and wrote the original draft.
Abdelhakim Dendouga: Validated the results and proofread the manuscript, editing it to enhance clarity, precision, and coherence.
Djamal Aouzellag: Contributed to document organization, validated the findings, and proofread the text to improve readability, rigor, and flow.

Received on November 6, 2024

REFERENCES

1. ***IEA, Renewables 2023 Analysis and forecasts to 2028.
2. G. Mayilsamy, S.R. Lee, Y.H. Joo, An improved model predictive control of back-to-back three-level NPC converters with virtual space vectors for high power PMSG-based wind energy conversion systems, ISA Transactions, **143**, 1 ,pp. 503–524 (2023).
3. M.H. Qais, H.M. Hasanien, S. Alghuwainem, A novel LMSRE- based adaptive PI control scheme for grid-integrated PMSG-based variable-speed wind turbine, International Journal of Electrical Power and Energy Systems, **125**, 1, pp. 106505 (2020).
4. T.Y. Heng, T.J. Ding, C.C.W. Chang, T. . Ping, H.C. Yian, M. Dahari, Permanent Magnet Synchronous Generator design optimization for wind energy conversion system: A review, 7th International Conference on Advances on Clean Energy Research, ICACER 2022, Barcelona, Spain, (2022).

5. M.A. Frikha, J. Croonen, K. Deepak, Y. Benômar, M. El Baghdadi, O. *Hegazy, Multiphase motors and drive systems for electric vehicle powertrains: State of the art analysis and future trends*, Energies, **16**, 2, pp. 768 (2023).
6. R. Bojoi, M.G. Neacsu, A. Tenconi, *Analysis and survey of multi-phase power electronic converter topologies for the more electric aircraft applications*, in Proc. International Symposium on Power Electronics, Electrical Drives, Automation and Motion Sorrento, Italy, pp. 440–445 (2012).
7. F. Scuiller, *Magnet shape optimization to reduce pulsating torque for a five-phase permanent-magnet low-speed machine*, IEEE Transactions on Magnetics, **50,** *4,* pp. 1–9 (2014).
8. S. Chekkal Ait Ouaret, Y. Imaouchen, D. Aouzellag, K.Ghedamsi, *A new modeling approach and comprehensive monitoring of electrical faults through spectral analysis in DSIM*, Periodica Polytechnica Electrical Engineering and Computer Science,**68**, *4*, pp. 344–355 (2024).
9. I. Gonzalez, M.J. Duran, H.S. Che, E. Levi, J. Aguado, *Fault-tolerant efficient control of six-phase induction generators in wind energy conversion systems with series parallel machine-side converters*, 7th IET International Conference on Power Electronics, Machines and Drives PEMD 2014, Manchester, UK (2014).
10. K.A. Chinmaya, G.K. Singh, *Modeling and experimental analysis of grid-connected six-phase induction generator for variable speed wind energy conversion system*, Electric Power Systems Research, **166**, *1*, pp. **151**–**162** (2019).
11. H.S. Che, W.P. Hew, N.A. Rahim, E. Levi, M. Jones, M.J. Duran, *Current control of a six-phase induction generator for wind energy plants,* 15th International Power Electronics and Motion Control Conference EPE/PEMC Novi Sad, Serbia (2012).
12. G.K. Singh, K. Nam, S.K. Lim*, A simple indirect field-oriented control scheme for multiphase induction machine*, IEEE Transactions on Industrial Electronics,**52**, *4*, pp. 1177–1184 (2005).
13. H.S. Che, M.J. Duran, W.P. Hew, N.A. Rahim, E. Levi, M. Jones*, Dc-link voltage balancing of six-phase wind energy systems with series-connected machine-side converters and NPC grid-side converter*, 38th Annual Conference on IEEE Industrial Electronics Society, IECON , Montreal, QC, Canada, (2012).
14. V. Yaramasu, B. Wu, P.C. Sen, S. Kouro, M. Narimani, *High-Power Wind Energy Conversion Systems: State-of-the-Art and Emerging Technologies,* IEEE Proceedings,103,12, pp. 2285–2301 (2015).
15. X. Peng, Z. Liu, D. Jiang, *A review of multiphase energy conversion in wind power generation*, Renewable and Sustainable Energy Reviews, **147**, *1*, pp. 111172 (2021).
16. M. Durán, S. Kouro, B. Wu, E. Levi, F. Barrero, S. Alepuz, *Six-phase PMSG wind energy conversion system based on medium-voltage multilevel converter*, 14th European conference on power electronics and applications, Birmingham (2011).
17. G. Estay, L. Vattuone, S. Kouro, M. Duran, B. Wu*, Dual-boost-NPC converter for a dual three-phase PMSG wind energy conversion system,* In Proceedings of the 2012 IEEE International Conference on Power Electronics, Drives and Energy Systems PEDES, Bengaluru, India (2012).
18. R.C. Portillo, M.A. Martín Prats, J.I. León, J.A. Sánchez, J.M. Carrasco, E. Galván, L. Garcia Franquelo*, Modeling strategy for back-to-back three-level converters applied to high-power wind turbines*, IEEE Transactions on Industrial Electronics, **53**, *5*, pp. 1483–1491 (2006).
19. S. Chennai, *Novel shunt active power filter based on nine-level NPC inverter using MC-LSPWM modulation strategy,* Rev. Roum. Sci. Techn.– Électrotechn. et Énerg., **69**, *1*, pp. 21–26 (2024).
20. Z. Zhang, F. Wang, J. Wang, J. Rodriguez, R. Kennel, *Nonlinear direct control for three-level NPC back-to-back converter PMSG wind turbine systems: Experimental assessment with FPGA*, IEEE Transactions on Industrial Informatics, **13**, *3,* pp. 1172–1183 (2017).
21. H. Xie, M. Novak, F. Wang, T. Dragicevic, J. Rodríguez, F. Blaabjerg, R. Kennel, M.L. Heldwein, *Cooperative Decision-making Approach for Multi-objective Finite Control Set Model Predictive Control without Weighting Parameters*, IEEE Transactions on Industrial Electronics**, 71**, *5*, pp. 4495–4506 (2024).
22. O.K. Krinah, R. Lalalou, Z. Ahmida, S. Oudina, *Performance investigation of a wind power system based on double-feed induction generator: Fuzzy versus proportional integral controller*s, Rev. Roum. Sci. Techn. – Électrotechn. et Énerg, **67,** *4*, pp. 403–408 (2022).
23. I. Yaichi, A. Semmah, P. Wira, *Control of doubly-fed induction generator using artificial neural network controller*, Rev. Roum. Sci. Techn. – Électrotechn. et Énerg**., 68**, *1*, pp. 46–51 (2023).
24. Y. Zhao, T.A. Lipo*, Space vector PWM control of dual three-phase induction machine using vector space decomposition*, IEEE Transactions on Industry Applications, **31***, 5*, pp. 742–749 (1995).
25. H. Zhang, G. Yao, L. Zhou, B. Mei, D. Li, *Sliding mode control based on six-phase PMSM speed control system*, IECON 2017 - 43rd Annual Conference of the IEEE Industrial Electronics Society, Beijing, China, (2017).
26. A.L. Eshkevari, M. Arasteh, *Model-Predictive Direct Power Control of Three-Phase Three-Level NPC PWM Rectifier*, in 8th Power Electronics, Drive Systems & Technologies Conference (PEDSTC 2017), Mashhad, Iran, (2017).
27. J. Rodríguez, J. Pontt, P. Cortés, R. Vargas, *Predictive Control of a Three-Phase Neutral Point Clamped Inverter*, IEEE Transactions on Industrial Electronics, **54**, *5*, pp. 2697–2705 (2007).
28. M. Benakcha, L. Benalia, A. Ammar, A. Bourek*, Wind Energy Conversion System Based on Dual Stator Induction Generator Controlled by Nonlinear Backstepping and PI Controllers*, Int. J. Syst. Assur. Eng. Manag, **8,** *1*, pp. 01–11, (2017).

29 K. Milev, V. Yaramasu, A. Dekka, S. Kouro*, Predictive control of multichannel boost converter and VSI-based six-phase PMSG wind energy systems with fixed switching frequency*, in Proc. IEEE 11th Power Electronics, Drive Systems, and Technologies Conference (PEDSTC), Tehran, Iran (2020).